Tribology International 153 (2021) 106563

Contents lists available at ScienceDirect

Tribology International

journal homepage: http://www.elsevier.com/locate/triboint

Friction of flat and micropatterned interfaces with nanoscale roughness

Saad Bin Jaber [a,b], Alex Hamilton [a], Yang Xu [a,*], Mehmet E. Kartal [c], Nikolaj Gadegaard [a], Daniel M. Mulvihill [a,*]

[a] James Watt School of Engineering, University of Glasgow, Glasgow, G12 8QQ, UK
[b] Department of Physics, College of Sciences, Al-Imam Mohammad Ibn Saud Islamic University (IMISU), Riyadh, 11623, Saudi Arabia
[c] School of Engineering, University of Aberdeen, Aberdeen, AB24 3UE, UK

ARTICLE INFO

Keywords:
Dry friction
Surface structure
Surface roughness

ABSTRACT

The dry friction of surfaces with nanoscale roughness and the possibility of using micropatterning to tailor friction by manipulating contact area is investigated. Square wave patterns produced on samples from silicon wafers (and their unstructured equivalent) were slid against unstructured silicon counter surfaces. The width of the square wave features was adjusted to vary the apparent feature contact area. The existence of nanoscale roughness was sufficient to ensure Amontons' first law ($F = \mu P$) on both structured & unstructured samples. Somewhat counterintuitively, friction was independent of the apparent feature contact area making it difficult to tailor friction via the feature contact area. This occurred because, even though the apparent feature contact area was adjusted, the surface roughness and nominal flatness at the contact interface was preserved ensuring that the *real* contact area and thereby the friction, were likewise preserved. This is an interesting special case, but not universally applicable: friction *can* indeed be adjusted by structuring provided the intervention leads to a change in real contact area (or interlocking)– and this depends on the specific surface geometry and topography.

1. Introduction

Friction is the mechanism responsible for transmitting tangential force across an interface when materials are in contact. The importance of friction is universal. Its role is obvious in situations such as tyre-on-road contact and wheel-on-rail contact or in mechanical components such as bearings and seals. However, it is also indirectly critical in the analysis of several kinds of systems. Examples include its influence on the vibration response of machinery [1,2], the control of mechanical systems [3,4] and even the structural behaviour of systems of aggregates and soils [5–8]. The mechanism by which friction is generated is complex and depends on a wide spectrum of factors including surface topography, material properties and surface chemistry. Even so, (for dry friction) much practical engineering design work still relies on the simple empirical laws published by Amontons [9] in 1699. The first is that friction force F is linearly proportional to the normal load P pressing the surfaces together:

$$F = \mu P, \tag{1}$$

with the proportionality constant μ being defined as the coefficient of friction (COF). The second is that friction is generally independent of nominal contact area. Despite their simplicity, these laws are very often a close enough approximation of reality to remain highly useful. They are also remarkably widely applicable across a large spectrum of materials and contact scenarios. In fact, we now have a reasonably satisfactory explanation for the origin of these laws. The first part of the explanation relates to contact area. Various experimental studies [10–13] have shown that, for real surfaces possessing surface roughness, the actual area in contact (or *real* contact area A_r) is usually very much less than the nominal contact area and, in many cases, is close to being linearly proportional to the normal load:

$$A_r = \kappa P \tag{2}$$

where κ is the proportionality constant. It is very important to note that Eq. (2) arises solely due to the multiscale random nature of surface roughness, provided that mating surfaces are linear elastic (Note: some researchers have reported a deviation from Amonton's law due to a nonlinear relation between real contact area and normal load [14]). The second part relates to how the friction force is generated on the real contact area. Bowden and Tabor [15] developed the idea that bonding interactions occur at the regions of real contact and that the friction force F is simply the force required to overcome the resulting (constant)

* Corresponding authors.
E-mail addresses: Yang.Xu@glasgow.ac.uk (Y. Xu), daniel.mulvihill@glasgow.ac.uk (D.M. Mulvihill).

https://doi.org/10.1016/j.triboint.2020.106563
Received 8 June 2020; Received in revised form 16 July 2020; Accepted 19 July 2020
Available online 25 July 2020

shear strength τ_s:

$$F = \tau_s A_r \tag{3}$$

Combining Eqs. (2) and (3) essentially produces the proportionality between normal load and friction which we know as Amontons' first law (Eq. (1)). For a given surface, regardless of nominal contact area, it is the normal load (only) which determines the real contact area and therefore, we can also deduce that friction must be independent of nominal contact area. Amontons' laws do not tell us how to predict the coefficient μ or give any indication of how we might control friction (a discussion of models attempting to predict μ is given in Ref. [16]). To accurately know the COF, it must usually be measured directly in a particular application. Ability to control dry friction is important since we very often require a specific level of optimal friction (e.g. in friction damping, in precision machine control or in dry bearings). Interestingly, the ability to vary and control friction can be used to improve the tactile experience and create a sense of 3D realism in touch technologies such as touch screens [17–19]. In theory, it may be possible to tailor the friction of rough surfaces by adjusting appropriate surface parameters. For example, numerical modelling in Hanaor et al. [20] revealed greater friction for surfaces exhibiting higher fractality. However, controlling and adjusting rough surface parameters (such as the fractal dimension) is extremely challenging in practice. A more easily achievable approach would be to use deterministic structured surfaces. Eq. (3) hints at one possible way forward: that of controlling friction via the real contact area A_r. Therefore, in this paper, we consider the possibility of structuring a surface to control friction via A_r.

Several studies have been carried out looking at using surface structuring to manipulate friction. Many of the structured surfaces in friction studies from the literature have been produced by laser surface texturing (LST) [21–26] and other techniques have included photolithographic etching [27,28], crystallization [29,30] and microcutting [31]. A comprehensive review of techniques and related friction studies is given in Gachot et al. [32]. Surface texturing has been shown to reduce friction in lubricated contacts by increasing hydrodynamic pressure [33], increasing lubricant film thickness [34] or providing lubricant reservoirs [35]. In contacts undergoing significant wear, texturing has been able to reduce friction [21,22] and wear rates [21,23] primarily via particle entrapment in surface grooves. Leaving aside the effect of wear on friction, studies on dry friction have been less conclusive. For example, surface structuring in Gachot et al. [24] was able to considerably reduce friction compared to the smooth interface reference case; but Kang et al. [36] measured a significant increase with their structured interfaces. However, the material pair and contact arrangement are all important here. The contact arrangement in Kang et al. [36] was a flat surface with aluminium micro-domes contacting a PDMS hemisphere. Here, the features may have been able to penetrate the soft PDMS and develop an increased contact area or some degree of interlocking. Whereas, the contact in Gachot et al. [24] involved two stiff steel surfaces (again ball-on-flat) both having microstructured channels. Interestingly, Gachot et al. noted a significantly lower friction when the channels on both surfaces were mutually perpendicular as compared to parallel. In a follow-on study [37] they attributed the difference to a reduced real contact area. Yu et al. [38] also studied the question of the friction anisotropy. This time for a smooth ball in contact with a grooved surface. They proposed that differences in friction due to the orientation of the grooves relative to the sliding direction were due to a combination of contact area, surface stiffness, stiction length and energy barrier effects. Another study indicating the somewhat inconclusive nature of the dry friction results is by Pettersson and Jacobson [39]. These authors had a smooth steel ball in reciprocating sliding contact with a square wave structured flat silicon surface having either a TiN or DLC coating. Compared to the flat (coated) surface benchmark, friction decreased only slightly for the structured surfaces having the TiN coating, but increased substantially for the structured surfaces with the DLC coating. The difference in behaviour was explained by the complicating influence of wear in each test type. In fact, the presence of wear in most of the dry friction work has made it difficult to distinguish the fundamental frictional response to the surface structure. We contend that (in the absence of wear) contact area is the key factor governing the influence of surface structure on friction and this is what we investigate in the present paper.

Reflecting on the structuring studies available in the friction literature, although many have been successful in creating nano- and microscale features on surfaces, controlling real contact area in any kind of accurate manner has rarely been possible. First, the structures produced by laser surface texturing have a high degree of irregularity making it impossible to guarantee a specific real contact area and second, very many of the friction studies have involved the ball-on-flat test arrangement which is problematic for a few reasons: the ball-on-flat has its own contact area versus load relation producing a contact area proportional to $P^{2/3}$, only a small number of the nano or micro features will make contact and each will make contact to a different extent – all of which makes it difficult to control the real contact area.

In this paper, our aim is to explore the possibility of tailoring friction based on contact area by creating structured interfaces where the percentage of nominal feature contact area is accurately known and controlled. Essentially, if the dependency of real contact area on normal load in Eq. (2) can be removed or minimised, it might be possible to control friction solely by adjusting A_r in Eq. (3). This requires a contact arrangement where the load versus contact area relationship is not affected by the overall feature or surface geometry – therefore, the flat-on-flat arrangement is preferable. Also, to minimise other dependencies of real contact area on normal load, it is important to minimise surface roughness and flatness. Finally, fabrication of features with a high level of fidelity to the design surface will be required. To meet these important requirements, photolithographic patterning and subsequent etching of silicon wafers is used to create a range of surfaces each with a different percentage nominal feature contact area. These are then tested to assess their impact on frictional behaviour and, especially, to determine if this approach can be used to tailor friction. Commercial silicon wafers are extremely flat and have roughness below 1 nm [40]. Therefore, it is also interesting to determine what kind of friction law is obeyed for both the structured and unstructured instances of these highly idealised surfaces.

2. Surface fabrication and friction testing

2.1. Surface fabrication and measurement

A square wave pattern was used for the structured silicon surfaces and the contact arrangement involved these samples in contact with a flat unstructured silicon sample. Commercial silicon wafers were used and an area of 10 × 10 mm^2 was structured. The microfabrication steps are summarized in Fig. 1. Patterned photoresist (positive tone, Microposit S1828) was realised using standard photolithography processes. Deep reactive ion etching (DRIE) using the Bosch process was then used to remove material in the exposed areas while guaranteeing near vertical sidewalls. Five different surface types were produced to give contact area ratios A_{nf}/A_n of 0.2, 0.4, 0.6, 0.8 and 1 where feature contact area ratio is defined as the total nominal (or apparent) feature contact area A_{nf} (i.e. the tops of the features) divided by the nominal area A_n (i.e. total enclosed planar area of 10 × 10 mm^2). The five surface types (in contact with the flat counter surface) are illustrated in Fig. 2. While the instance with a contact area ratio of unity is simply an unstructured silicon wafer surface, the four structured cases were produced by holding the period constant at 100 μm and varying the ratio of the period occupied by the feature. A feature depth d of approximately 70 μm was used for all structured samples. An SEM image of one of the structured surfaces ($A_{nf}/A_n = 0.2$) is given in Fig. 3. Following fabrication, all surfaces were cleaned in an ultrasonic bath using acetone and isopropanol for 5 min, rinsed in RO water and then blow dried using a nitrogen gun. Surface topography was then analysed using an Icon

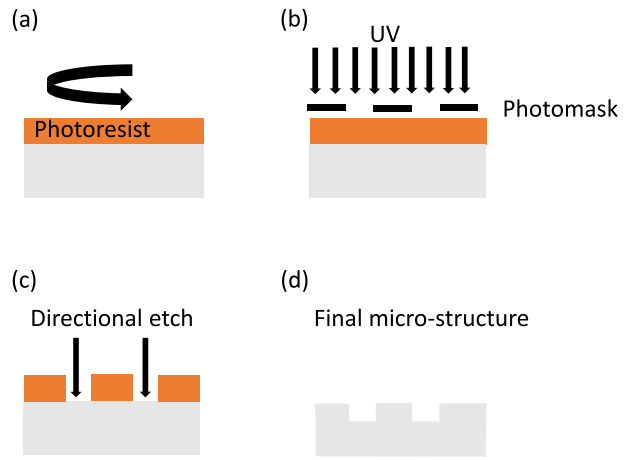

Fig. 1. Photolithographic etching steps for structured surface fabrication.

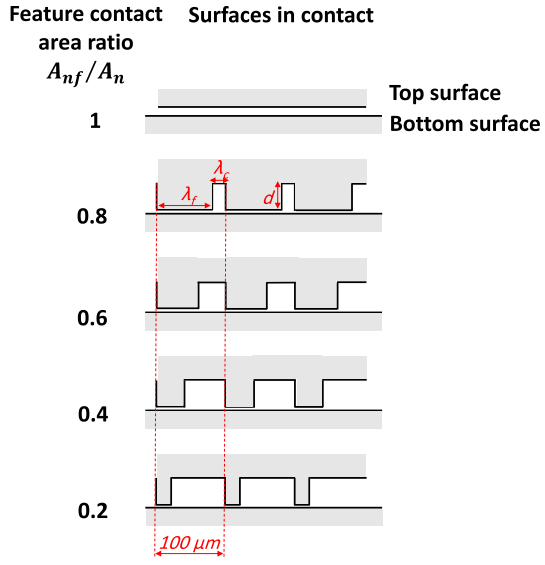

Fig. 2. Schematic representation of feature contact area ratios. Feature contact area ratio $A_{nf}/A_n = \lambda_f/(\lambda_f + \lambda_c)$.

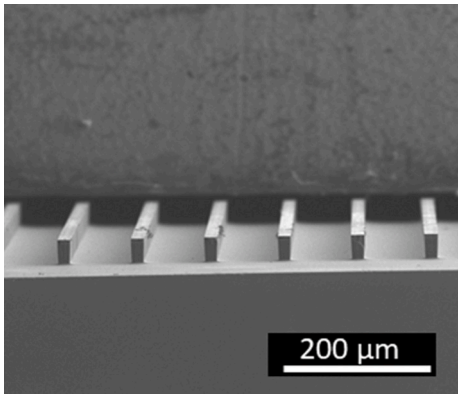

Fig. 3. SEM image of a structured surface having a contact area ratio A_{nf}/A_n of 0.2.

atomic force microscope (AFM) (Bruker, USA). Scans (500 × 500 nm) were taken on both the structured and unstructured surfaces (for the structured surfaces, the scans were taken on the tops of the features). For each sample, scans were performed at five different locations both before and after the friction tests. Root mean square roughness (Rq) values taken from these scans were then averaged among samples of the same contact area ratio.

2.2. Friction testing

A bespoke friction test rig was designed for the experiments. The rig is similar to the 'sled type' friction test in ASTM D1894 [41]. Fig. 4 shows a 3D rendered model of the rig (right) with an inset schematic (left) showing the detail around the contact interface (the numbers indicate key components). The interface under investigation (denoted by the blue arrow in Fig. 4) consists of a 10 × 10 mm^2 upper silicon sample (1) contacting a 25 mm long (15 mm wide) lower silicon sample (2). The upper sample was either structured or flat (depending on the test) and the lower sample was always flat and unstructured. The back surfaces of the upper and lower test samples were glued to upper and lower backing plates (3) and (4). Normal load P was applied to the contact by tightening nuts on four compression springs pressing against an upper arm (5). The load is then transmitted to the upper backing plate through a 110 N miniature button load cell (6) for accurate measurement. The button load cell (LBS, Interface Force Measurements, UK) has a spherical tip allowing the upper specimen to self-align with the lower specimen (an important requirement to ensure the conformity of surfaces in flat-on-flat contact). The mechanism maintained an almost constant normal load during sliding although we note that others (Senetakis and Coop [42]) have used a force controlled stepper motor to fix a target normal load. Tangential load is applied to the lower backing plate via a connecting rod (7) attached to a motorised stage (8). The lower backing plate is free to slide on a very low friction linear bearing (9). Tangential load F is measured via a 110 N universal tension/compression load cell (SML, Interface Force Measurements, UK) (10) connected in-line with the connecting rod. As the lower specimen slides, stoppers (11) prevent sliding of the upper specimen.

To eliminate frictional instabilities and allow the friction results to reach a steady state [43], a run-in protocol was carried out involving 10 mm of sliding at the maximum load of 50 N. The surfaces were then returned to the initial starting position. Normal load was then stepped up (from zero) in increments of 5 N. At each increment, the normal load was held fixed and 0.5 mm of sliding was carried out at an average speed of 0.02 mm/s. After each increment, normal load was increased from its present value and sliding was continued from the current position. This was continued for nine increments up to a maximum load of 50 N corresponding to a total travel distance of 4.5 mm. Note that, for the structured specimens, the longitudinal direction of the features was parallel to the sliding direction. A LabVIEW program was written to control the motorised stage and log the data. Signals from the load cells were first passed through a NI-9237 full bridge amplifier (National Instruments, UK) before being passed to the PC. A displacement signal was taken directly from the motor's control software. Five repeat tests (with new specimens each time) were carried out on each feature contact area instance (0.2, 0.4, 0.6, 0.8 and 1).

3. Results and discussion

Table 1 shows the mean RMS surface roughness of the samples before and after testing. Prior to testing, RMS roughness was in the range 1.2–2.3 nm which is very much at the lower limit of roughness for the processing and fabrication of surfaces in general. Following testing, the roughness values reduced slightly. This is likely due to some degree of wear during running-in and during the test itself.

Fig. 5 shows representative plots of tangential force versus displacement for each feature contact ratio instance. Most of the curves exhibit a clearly defined static friction peak followed by relatively constant sliding friction. Each graph plots tangential force for five normal loads. Note that each 10 N increase in normal load, produces roughly equal step increases in friction force suggesting a near linear

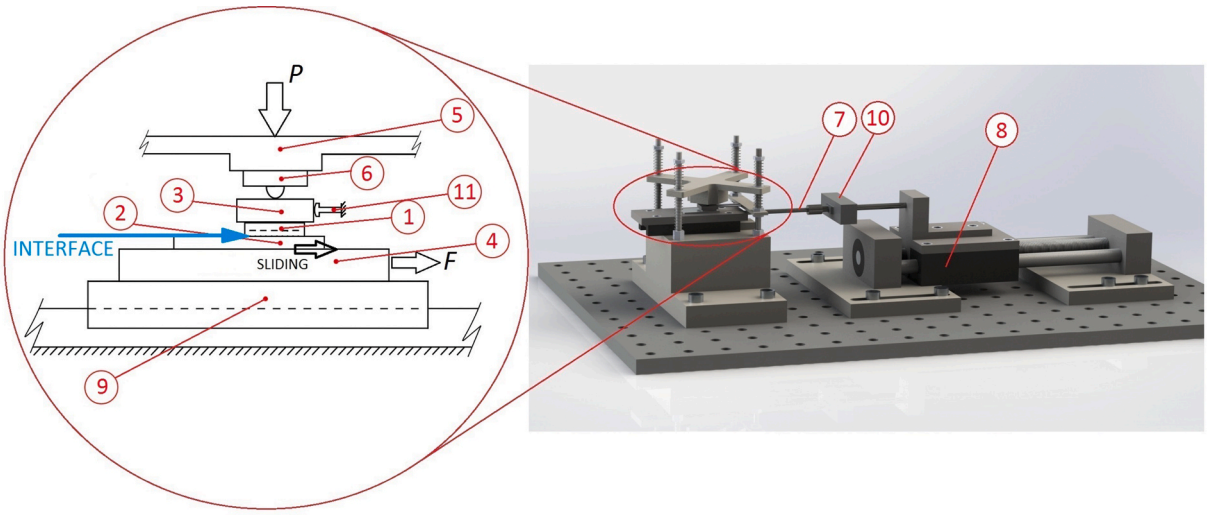

Fig. 4. Schematic of the experimental 'sled type' friction rig: (1) Upper silicon specimen, (2) Lower silicon specimen (always flat), (3) Upper backing plate, (4) Lower backing plate, (5) Upper arm, (6) Miniature button load cell, (7) Connecting rod, (8) Linear stage and motor, (9) Low friction linear bearing, (10) Tension/compression load cell and (11) Stoppers. (For interpretation of the references to colour in this figure legend, the reader is referred to the Web version of this article.)

Table 1
Mean RMS surface roughness *Rq* before and after testing. Roughness values are the mean of five different AFM scans per sample for each of the five repeat tests (i.e. mean of 25 measurements). Bracketed values are standard deviations.

Feature contact area ratio	RMS Roughness *Rq* (nm)	
	Before	After
0.2	1.8 (0.5)	1.1 (0.5)
0.4	2.1 (1.2)	1.2 (1.3)
0.6	2.3 (0.6)	1.0 (0.5)
0.8	2.1 (0.6)	1.2 (0.2)
1	1.2 (0.9)	0.6 (0.2)

relationship. This is evident from Fig. 6a (static friction force versus normal load) which clearly indicates linearity. It follows that the coefficient of static friction μ is roughly independent of normal load (Fig. 6b). Fig. 6 essentially confirms, that despite their very low nanoscale roughness, all of the surfaces tested (flat or micropatterned) obey Amontons' description $F = \mu P$. Note that the static friction force was defined as the maximum tangential force on the static friction peak. Of course, it should also be noted that, as tangential force increases on the pre-sliding contact, asperity contacts progressively transition from stick to slip [5,44]. So, the point at which static friction is measured actually represents the limiting tangential force at the point of transition from this mixed regime to full sliding – this is the usual approach to defining the macroscopic static friction force.

The question remains as to whether we can manipulate or tailor friction by adjusting feature contact area. Fig. 7 plots the coefficient of static friction against feature contact area ratio (A_{nf}/A_n). Note, that for feature contact area ratios 0.4, 0.6 and 0.8, the coefficient of friction is roughly independent of feature contact area and constant at about $\mu = 0.4$. There are two outliers in that the results for ratios 0.2 and 1 lie slightly above and below this value. However, it is likely that the differences here are not attributable to the contact area ratio, but to other factors. For example, the $A_{nf}/A_n = 1$ case is a flat unstructured silicon wafer that has not been subjected to the fabrication process described in Section 2.1 and, although the structured surfaces were subject to a clearing procedure, it is probable that processing introduces some minor residual surface topography changes (e.g. tiny adhered particles, feature edge effects etc.). For the $A_{nf}/A_n = 0.2$ outlier (which *will* have been through fabrication), it is still possible that some differences in surface topography of the feature surfaces existed for the samples tested. Certainly, there is no evidence of any significant dependency between (nominal) feature contact area and friction. The obvious implication of this is that manipulating or tailoring friction via feature contact area is largely ruled out in this case.

So why might friction be independent of feature contact area? We return to what we know about friction and rough surface contact. Bowden and Tabor's formula in Eq. (3) tells us that friction is given by interfacial shear strength times real contact area (i.e. $F = \tau_s A_r$). Essentially, the behaviour of A_r will be indicative of F. However, the real contact area is difficult to determine experimentally (especially for opaque specimens with nanoscale roughness), but we can estimate it (for our experimental surfaces) using well established modelling approaches. Here we use both the asymptotic Bush, Gibson and Thomas (BGT) model [45] and a numerical model based on the Boundary Element Method (BEM) [46,47] to estimate the real contact areas. The BGT model assumes that the rough surfaces are in purely normal contact over the peaks of semi-ellipsoidal asperities. When normal load is nearly vanishing, an asymptotic linear relation between the real contact area and normal load is obtained [31]. Therefore, the asymptotic BGT is valid for lightly loaded elastic contacts such as the one in our experiments. According to the BGT model, the real area of contact A_r (as a fraction of the nominal area A_n) is given by:

$$\frac{A_r}{A_{nf}} = \frac{\kappa}{\sqrt{|\nabla h|^2}} \frac{\overline{p}}{E^*} \tag{4}$$

where κ (different to the κ in Eq. (2)) is a proportionality constant given by $\sqrt{2\pi}$, $\sqrt{|\nabla h|^2}$ is the root mean square (RMS) of the rough surface gradient, $\overline{p}$ is the average pressure over the nominal feature contact area A_{nf} and E^* is the effective Young's modulus of the contact pair. The key term to identify here is the RMS rough surface gradient (the others are constants) and this was determined directly from the AFM surface topography scans. A_r was calculated from Eq. (4) for each surface scan and a single mean value was then produced for each contact ratio category. The A_r calculation was done at the normal pressure $\overline{p}$ corresponding to the maximum normal load in the experiments (50 N). The resulting estimation of real contact area is plotted against feature contact area ratio in Fig. 8a. A similar estimate was carried out using the BEM model. Here the entire surface was imported into a well validated open source BEM rough surface contact solver (https://contact.engineering [46,47]) to calculate A_r. A mean value was determined for each feature contact area instance based on the 25 available scans. The

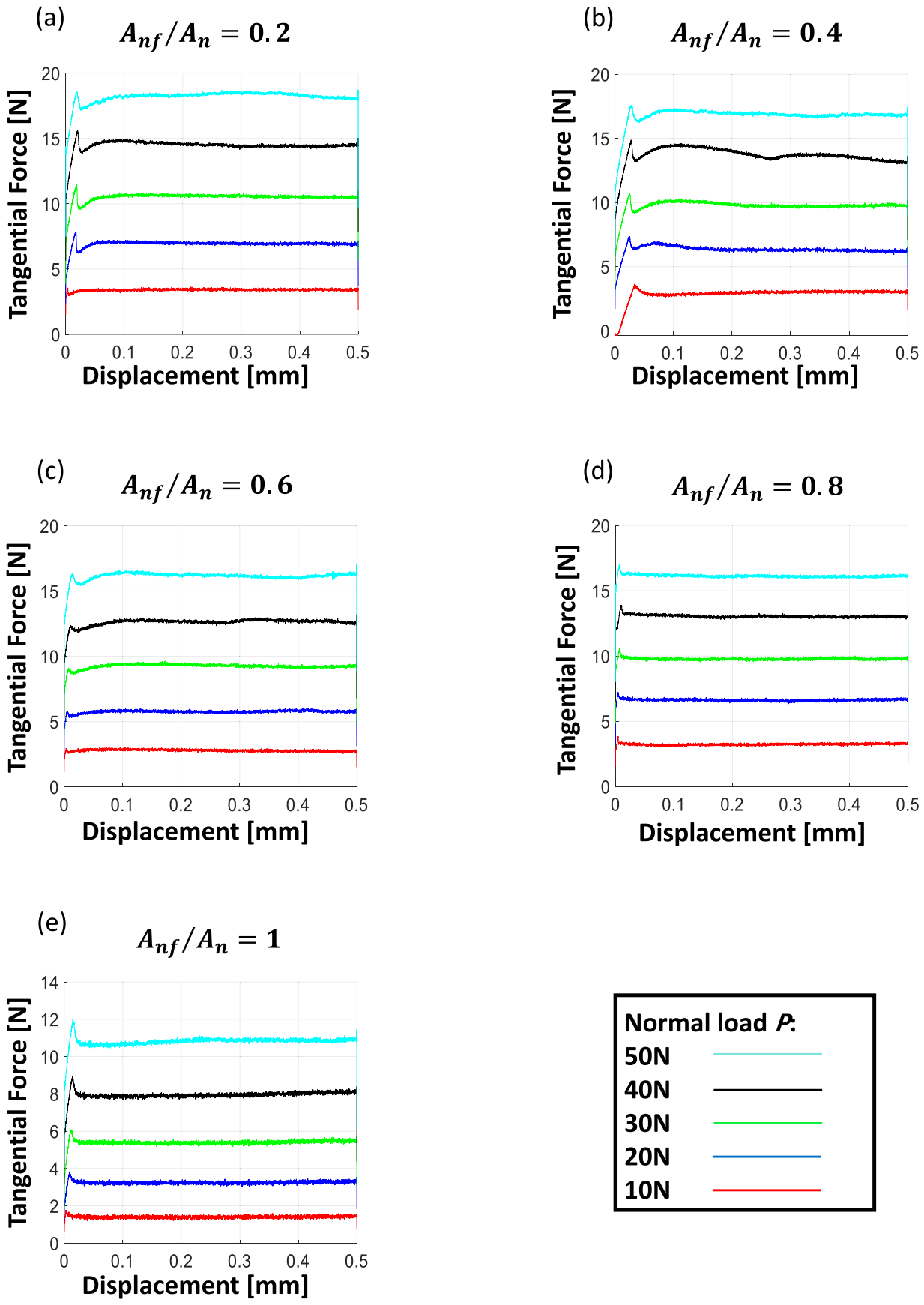

Fig. 5. Representative tangential force versus displacement plots for surfaces having feature contact area ratios (A_{nf}/A_n) of: (a) 0.2, (b) 0.4, (c) 0.6, (d) 0.8 and (e) 1. Each plot shows the effect of varying the normal load P (see legend).

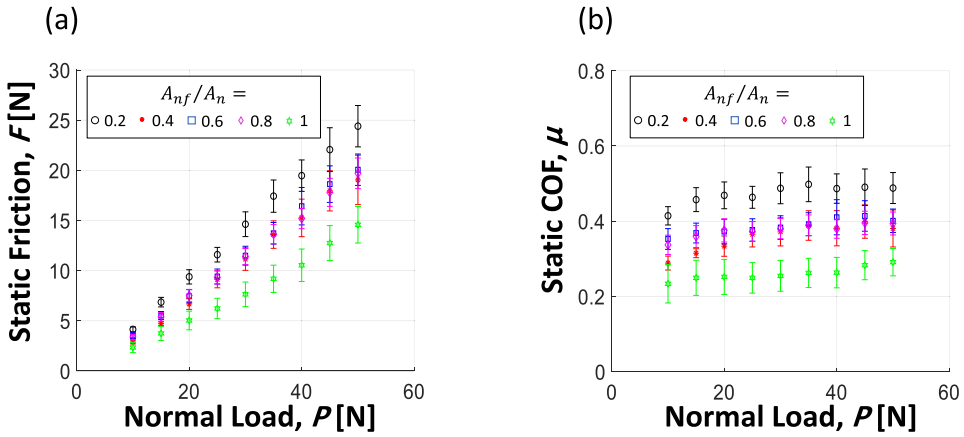

Fig. 6. (a) Static friction force F versus normal load P (for all feature contact area instances) and (b) coefficient of static friction f versus normal load P (also for all feature contact area instances). Feature contact area ratio (A_{nf}/A_n) is given in the legend.

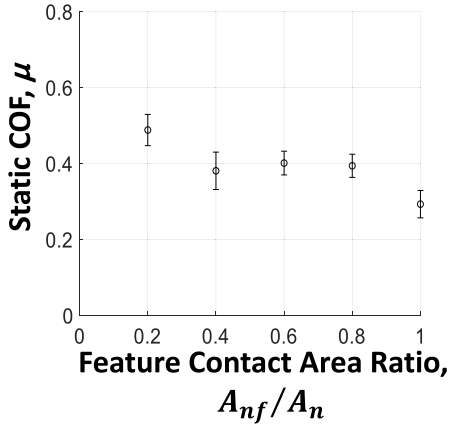

Fig. 7. Coefficient of static friction f versus feature contact area ratio (A_{nf}/A_n).

corresponding result is plotted in Fig. 8b.

Encouragingly, both approaches predict a very similar result and we can also see that the A_r follows a similar trend (with feature contact area) as the friction results in Fig. 7. That is, A_r is roughly independent of feature contact area apart from the lower value outlier (discussed later) at $A_{nf}/A_n = 1$. Therefore, the distinction between real contact area A_r and feature nominal contact area A_{nf} is critical. Although we have varied A_{nf}, the real contact area A_r remains roughly unchanged. Thus, adjusting the feature contact area here (even on the micron scale) is simply similar to adjusting the macroscopic nominal contact area A_n and we know from Amonton's law that friction is independent of nominal contact area. The reason why we have a load dependent, nominal area independent result in agreement with Amontons is simply because of the inevitable presence of surface roughness on the flat surface tops of the features. The load-area relationship in Eq. (2) tells us that A_r depends only on the normal load P and not on nominal contact area $A_n$or A_{nf}. However, this applies only if changes in nominal contact area preserve the same surface topography as is the case as we adjust the nominal feature area (i.e. the tops of the features always have the same surface topography). Thus, Eq. (2) applies to the structured surfaces (even with nanoscale roughness) and the overall result is again Amontons' simple relationship in Eq. (1). Amontons also holds for the flat surfaces. It is worth pausing to note that the applicability of Amontons' laws across the roughness length scales is rather remarkable. If one envisages perfectly flat surfaces with zero roughness, then the load dependency in Eq. (2) would not apply, Amontons' law would not hold, and according to Eq. (3), friction could then be manipulated by adjusting feature contact area. However, a perfectly smooth surface is impossible in practice and it would appear that roughness at any scale may be sufficient to lead to Amontons' relationship. We should note, that we are not making the general conclusion that friction cannot be manipulated by structuring surfaces –

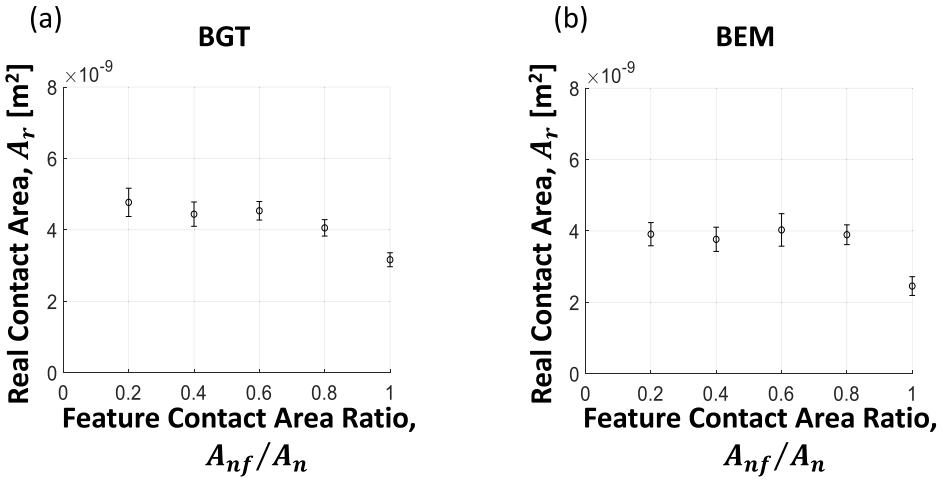

Fig. 8. Predicted real area of contact A_r versus feature contact area ratio (A_{nf}/A_n) as estimated by (a) the BGT model and (b) the BEM method. Normal load $P = 50$ N. Nominal areas (i.e. 10 × 10 mm^2) and feature areas etc. are the same as for the experimental specimen.

indeed others such as Gachot et al. [24] have been able to alter dry friction in this way. The possibilities will actually depend on the specific surface topographies involved. The structured surfaces in our work were highly idealised square wave patterns produced on highly flat surfaces with nanoscale roughness. Therefore, when the surfaces were patterned, the tops of the features retained the same surface topography (and flatness) leading to a friction response independent of nominal feature contact area. In Gachot et al. [24], laser structuring was used which will completely alter the original surface roughness and the roughness on the features will be different from the original nominally flat roughness. Thus, friction can be expected to vary according to the different topographies imparted. Also, when feature interlocking is present, the ploughing mechanism of friction (plastic deformation of asperities) [15] will be more dominant and again feature size may play a role. The outlier point (at $A_{nf}/A_n = 1$) in Fig. 8 is interesting as the friction results in Fig. 7 exhibit the same trend for $A_{nf}/A_n = 1$. This suggests that there are differences in surface topography between the unstructured and structured surfaces (tops of the features) which leads to the observed friction difference – but, as noted earlier, this difference in topography is likely due to the fact that (unlike the unstructured surface) the structured surface has been subjected to a number of processing steps.

4. Conclusions

This paper investigates the dry friction of surfaces with nanoscale roughness and investigates the possibility of using micropatterning to tailor contact area and thereby friction. Commercial silicon wafers were used owing to their high flatness and low roughness (Rq: 0.6–2.3 nm here). Nominally flat structured interfaces with a square wave pattern were fabricated using standard lithographic etching. The structured surfaces were then slid against a flat unstructured silicon counter surface. Keeping the period of the square wave constant at 100 μm, different instances of the pattern were fabricated having different feature widths in order to vary the feature contact area ratio between 0.2 and 1 (unity being equivalent to an unstructured surface).

Results indicate that both structured and unstructured surfaces obeyed Amontons' linear load dependence: $F = \mu P$. In addition, the results (somewhat counterintuitively) show a friction force largely independent of feature contact area making it largely impossible (in this case) to use feature contact area as a means to control friction. The reason for this load dependent, area independent result has been established: the nanoscale surface roughness present on both the structured and unstructured surfaces dictates the response. The patterning varied the magnitude of the feature contact area, but preserved the same surface topography. This leads to real contact area being dependent only on the normal load and not on the total apparent (or nominal) area in contact. For a fixed normal load, the BGT and BEM approaches were used to estimate real contact area and both confirmed near independence with feature contact area ratio. Essentially, the nominal feature contact area (for the structured interfaces) behaves exactly like the nominal area in Amonton's second law which describes friction as independent of nominal contact area. It is interesting in itself that Amontons' laws apply to the structured and unstructured instances of these surfaces with nanoscale roughness and it demonstrates their wide applicability across roughness length scales.

Finally, returning to the question of tailoring friction. The fact that the structuring (and varying of feature contact area) in this work cannot be used to effectively tailor friction is not a generally applicable conclusion. The surfaces in this work are highly idealised and, crucially, preserve essentially the same surface roughness on a flat plane as the apparent contact area is adjusted. This is an important subtlety. Indeed, we have pointed to previous studies [24] were structuring *has* been shown to adjust friction levels. Ability to tailor friction requires the ability to adjust the total *real* contact area of the interface and this will be possible with certain surfaces and contact configurations (for example, adjusting the wavelength of a sine wave surface can be expected to vary real contact area based on the contact mechanics of the surface geometry [48]). Thus, effectiveness in tailoring friction will depend on the specific surface geometry and topography of an interface. Finally, we should point out that the somewhat idealised case highlighted in the present study may possibly have applications were it is necessary to maintain a certain friction level, but considerably reduce the size of the nominal contact area (for example, were channels are required to increase heat transfer from a sliding contact).

CRediT authorship contribution statement

Saad Bin Jaber: Methodology, Software, Validation, Formal analysis, Visualization, Investigation. **Alex Hamilton:** Methodology, Resources. **Yang Xu:** Conceptualization, Supervision, Writing - review & editing. **Mehmet E. Kartal:** Conceptualization, Supervision, Writing - review & editing. **Nikolaj Gadegaard:** Supervision, Writing - review & editing. **Daniel M. Mulvihill:** Supervision, Conceptualization, Writing - original draft, Writing - review & editing, Project administration, Funding acquisition.

Declaration of competing interest

The authors declare that they have no known competing financial interests or personal relationships that could have appeared to influence the work reported in this paper.

Acknowledgements

The authors would like to acknowledge the support of the Leverhulme Trust for funding the work via project grant "Fundamental Mechanical Behaviour of Nano and Micro Structured Interfaces" (RPG-2017-353). EPSRC support (for AH) is also acknowledged via an EPSRC-DTP studentship (EP/N509668/1). We would also like to thank the technical staff at the James Watt Nanofabrication Centre (JWNC) for assistance in fabricating the structured Si samples. The authors also acknowledge the assistance of Ms Sarah Fontana in producing the 3D solid model in Fig. 4. Finally, S.B-J acknowledges the support of the Saudi Arabian Cultural Bureau in London and Al-Imam Mohammad Ibn Saud Islamic University (IMISU), Riyadh for sponsoring and supporting his PhD studies.

References

[1] Sever IA. Experimental validation of turbomachinery blade vibration predictions. PhD. Dissertation. Imperial College London; 2004.
[2] Chen G, editor. 4 - friction–vibration interactions," handbook of friction-vibration interactions. Woodhead Publishing; 2014. p. 153–305.
[3] Friedland B, Park Y. On adaptive friction compensation. IEEE Trans Automat Contr 1992;37(10):1609–12.
[4] Rymuza Z. Control tribological and mechanical properties of MEMS surfaces. Part 1: critical review. Microsyst Technol 1999;5(4):173–80.
[5] Kasyap SS, Senetakis K. Experimental investigation of the coupled influence of rate of loading and contact time on the frictional behavior of quartz grain interfaces under varying normal load 2019;19(10):4019112.
[6] Sandeep CS, Senetakis K. Grain-scale mechanics of quartz sand under normal and tangential loading. Tribol Int 2018;117:261–71.
[7] Sandeep CS, Senetakis K. An experimental investigation of the microslip displacement of geological materials. Comput Geotech 2019;107:55–67.
[8] Sandeep CS, Senetakis K. Effect of young's modulus and surface roughness on the inter-particle friction of granular materials. Materials 2018;11(2):217.
[9] Amontons G. De la résistance causée dans les machines. Mémoires de l'Académie Royale A 1699:257–82.
[10] Bowden FP, Tabor D. The area of contact between stationary and between moving surfaces. Proc Roy Soc Lond Math Phys Sci 1939;169(938):391–413.
[11] Bennett AI, Harris KL, Schulze KD, Urueña JM, McGhee AJ, Pitenis AA, Müser MH, Angelini TE, Sawyer WG. Contact Measurements of randomly rough surfaces. Tribol Lett 2017;65(4):134.
[12] Hendriks CP, Visscher M. Accurate real area of contact Measurements on polyurethane. J Tribol 1995;117(4):607–11.
[13] Helseth LE. Optical force sensing principle based on transparent elastomer with a rough surface. Sensor Actuator Phys 2017;263:667–76.

[14] Weber B, Suhina T, Junge T, Pastewka L, Brouwer AM, Bonn D. Molecular probes reveal deviations from Amontons' law in multi-asperity frictional contacts. Nat Commun 2018;9(1):888.
[15] Bowden FP, Tabor D. The friction and lubrication of solids. Oxford: Clarendon Press; 1950.
[16] Mulvihill DM, Kartal ME, Nowell D, Hills DA. An elastic–plastic asperity interaction model for sliding friction. Tribol Int 2011;44(12):1679–94.
[17] Kim S-C, Israr A, Poupyrev I. Tactile rendering of 3D features on touch surfaces. In: Proceedings of the 26th annual ACM symposium on User interface software and technology. St. Andrews, Scotland, United Kingdom: Association for Computing Machinery; 2013. p. 531–8.
[18] Levesque V, Oram L, MacLean K, Cockburn A, Marchuk N, Johnson D, Colgate JE, Peshkin M. Frictional widgets: enhancing touch interfaces with programmable friction. In: CHI '11 extended abstracts on human factors in computing systems. Vancouver, BC, Canada: Association for Computing Machinery; 2011. p. 1153–8.
[19] Childs THC, Henson B. Human tactile perception of screen-printed surfaces: self-report and contact mechanics experiments. Proc IME J J Eng Tribol 2007;221(3):427–41.
[20] Hanaor DAH, Gan Y, Einav I. Static friction at fractal interfaces. Tribol Int 2016;93:229–38.
[21] Xing Y, Deng J, Feng X, Yu S. Effect of laser surface texturing on Si3N4/TiC ceramic sliding against steel under dry friction. Mater Des 2013;52:234–45. 1980-2015.
[22] Borghi A, Gualtieri E, Marchetto D, Moretti L, Valeri S. Tribological effects of surface texturing on nitriding steel for high-performance engine applications. Wear 2008;265(7):1046–51.
[23] Sun Q, Hu T, Fan H, Zhang Y, Hu L. Dry sliding wear behavior of TC11 alloy at 500°C: influence of laser surface texturing. Tribol Int 2015;92:136–45.
[24] Gachot C, Rosenkranz A, Reinert L, Ramos-Moore E, Souza N, Müser MH, Mücklich F. Dry friction between laser-patterned surfaces: role of alignment, structural wavelength and surface chemistry. Tribol Lett 2013;49(1):193–202.
[25] Rosenkranz A, Reinert L, Gachot C, Mücklich F. Alignment and wear debris effects between laser-patterned steel surfaces under dry sliding conditions. Wear 2014;318(1):49–61.
[26] Etsion I. State of the art in laser surface texturing. J Tribol 2005;127(1):248–53.
[27] Echávarri Otero J, de la Guerra Ochoa E, Bellón Vallinot I, Chacón Tanarro E. Optimising the design of textured surfaces for reducing lubricated friction coefficient 2017;29(3):183–99.
[28] Xu Y, Yu J, Geng J, Abuflaha R, Olson D, Hu X, Tysoe WT. Characterization of the tribological behavior of the textured steel surfaces fabricated by photolithographic etching. Tribol Lett 2018;66(2):55.
[29] Nair RP, Zou M. Surface-nano-texturing by aluminum-induced crystallization of amorphous silicon. Surf Coating Technol 2008;203(5):675–9.
[30] Zou M, Cai L, Wang H, Yang D, Wyrobek T. Adhesion and friction studies of a selectively micro/nano-textured surface produced by UV assisted crystallization of amorphous silicon. Tribol Lett 2005;20(1):43–52.
[31] Shimizu J, Nakayama T, Watanabe K, Yamamoto T, Onuki T, Ojima H, Zhou L. Friction characteristics of mechanically microtextured metal surface in dry sliding. Tribol Int 2019:105634.
[32] Gachot C, Rosenkranz A, Hsu SM, Costa HL. A critical assessment of surface texturing for friction and wear improvement. Wear 2017;372–373:21–41.
[33] Etsion I, Burstein L. A model for mechanical seals with regular microsurface structure. Tribol Trans 1996;39(3):677–83.
[34] Costa HL, Hutchings IM. Hydrodynamic lubrication of textured steel surfaces under reciprocating sliding conditions. Tribol Int 2007;40(8):1227–38.
[35] Spencer A. Optimizing surface texture for combustion engine cylinder liners,"Licentiate thesis, comprehensive summary. Luleå: Luleå tekniska universitet; 2010.
[36] Kang M, Park YM, Kim BH, Seo YH. Micro- and nanoscale surface texturing effects on surface friction. Appl Surf Sci 2015;345:344–8.
[37] Prodanov N, Gachot C, Rosenkranz A, Mücklich F, Müser MH. Contact mechanics of laser-textured surfaces. Tribol Lett 2013;50(1):41–8.
[38] Yu C, Yu H, Liu G, Chen W, He B, Wang QJ. Understanding topographic dependence of friction with micro- and nano-grooved surfaces. Tribol Lett 2014;53(1):145–56.
[39] Pettersson U, Jacobson S. Influence of surface texture on boundary lubricated sliding contacts. Tribol Int 2003;36(11):857–64.
[40] Teichert C, MacKay JF, Savage DE, Lagally MG, Brohl M, Wagner P. Comparison of surface roughness of polished silicon wafers measured by light scattering topography. Soft x-ray Scatter. Atomic Force Micro. 1995;66(18):2346–8.
[41] ASTM D1894-14. Standard test method for static and kinetic coefficients of friction of plastic film and sheeting. West Conshohocken, PA: ASTM International; 2014.
[42] Senetakis K, Coop M. The development of a new micro-mechanical inter-particle loading apparatus. Geotech Test J 2014;37(6):1028–39.
[43] Dillavou S, Rubinstein SM. Nonmonotonic aging and memory in a frictional interface. Phys Rev Lett 2018;120(22):224101.
[44] Mergel JC, Sahli R, Scheibert J, Sauer RA. Continuum contact models for coupled adhesion and friction. J Adhes 2019;95(12):1101–33.
[45] Bush AW, Gibson RD, Thomas TR. The elastic contact of a rough surface. Wear 1975;35(1):87–111.
[46] Polonsky IA, Keer LM. A numerical method for solving rough contact problems based on the multi-level multi-summation and conjugate gradient techniques. Wear 1999;231(2):206–19.
[47] Pastewka L, Sharp TA, Robbins MO. Seamless elastic boundaries for atomistic calculations. Phys Rev B 2012;86(7):75459.
[48] Johnson KL. Contact mechanics. Cambridge: Cambridge University Press; 1985.